JOM, Vol. 65, No. 7, 2013
DOI: 10.1007/s11837-013-0614-3

Electroplated Bimagnetic Microwires: From Processing to Magnetic Properties and Sensor Devices

JACOB TORREJÓN,[1,2,5] GERMÁN INFANTE,[1,3] GIOVANNI BADINI-CONFALONIERI,[1] KLEBER R. PIROTA,[1,4] and MANUEL VÁZQUEZ[1]

1.—Institute for Materials Science, CSIC, 28049 Madrid, Spain. 2.—*Present address:* National Institute for Materials Science, Tsukuba 305-0047, Japan. 3.—IMDEA Materials, 28906 Madrid, Spain. 4.—Instituto de Física Gleb Wataghin, University Estadual Campinas, UNICAMP, Campinas, SP 13083970, Brazil. 5.—e-mail: torrejondiaz.jacob@nims.go.jp

Multilayer microwires with biphase magnetic behavior are revisited in this work. They are fabricated by the combination of ultrarapid solidification and electroplating techniques, and they are composed by ferromagnetic nucleus, intermediate glass layer, and ferromagnetic outer shell. Different magnetic configurations have been explored: soft/hard (CoFeSiB/CoNi and FeSiB/CoNi), soft/soft (CoFeSiB/FeNi), and hard/soft (FePtSi/FeNi). Their magnetic properties are mainly determined by the magnetic interactions between both magnetic phases: (I) a magnetoelastic coupling that arises from the mechanical stresses induced during the growth of the external magnetic shell and (II) a magnetostatic bias field that arises from uncompensated magnetic charges of the hard layer. Most outstanding static (i.e., low-field hysteresis loops) and dynamic (i.e., magnetoimpedance and ferromagnetic resonance) properties are reviewed in this article. The possibility to tailor the magnetization reversal of the soft phase through the tuning of those magnetic couplings places multilayer biphase microwires in a very competitive position as functional sensing elements suitable for a number of technological applications. In particular, we focus on their use in multifunctional sensor devices and fluxgate applications.

INTRODUCTION

Ferromagnetic amorphous metals have been investigated for several decades because of their outstanding magnetic behavior mostly as very soft materials that make them especially suitable as sensing elements in technologies and devices.[1] Their outstanding magnetic behavior is a consequence of the intrinsic atomic disordering that gives rise to quite interesting fundamental phenomena.[2] Glassy metals are prepared by several rapid solidification techniques that enable their preparation in the shape of ribbons or wires.[3] Amorphous magnetic alloys can be also prepared as bulk material[4] or can give rise to ultrasoft alloys after suitable thermal treatments resulting in nanocrystallization.[4,5]

Amorphous magnetic wires show some specific characteristics deriving from the symmetry of their cylindrical shape. They are currently prepared by two different techniques: (I) in-rotating water quenching (100–150 μm diameter) and (II) by quenching and drawing (0.1–30 μm diameter) in which case they are covered by a Pyrex coating. The microwires with larger diameter were studied in detail during the 1980s showing fascinating magnetic effects: large Barkhausen discontinuity, very high permeability level for ultrasoft alloys, single domain wall (DW) propagation, giant magnetoimpedance (GMI), and stress impedance (SI).[3] In the last 25 years, the research interest has been mainly focused on thinner glass-coated microwires (GCMs)[3,5–7] because of several reasons: (I) Their magnetic properties can be tailored by the fabrication and subsequent processing, (II) their geometry and composition can be also tuned by the fabrication parameters, (III) they can be considered nearly ideal systems for fundamental and micromagnetic studies, (IV) their dynamic properties at high frequency range (GMI and ferromagnetic resonance [FMR]), and (V) their promising technological applications

(Published online April 26, 2013)

in electronic devices as sensing element (see Ref. 8 and references therein).

While planar multilayer structures have been investigated for years, much less attention has been paid to cylindrical-symmetry multilayered systems. Multilayered microwires have been introduced employing any of these two families of amorphous wire precursor. In the former case, the additional metallic layer is directly electroplated onto the surface of metallic nucleus.[9–11] This process can be achieved also starting form ribbon-shaped samples.[12,13] The process in the case of glass-coated microwires is more complex and it requires further step, where noble metal is sputtered onto the glass to act as electrode in the subsequent electroplating.[14,15] However, the insulated multilayer microwire (MM) presents more interesting properties in terms of magnetic couplings, and the electrical insulation between the two metallic layers is very convenient for technological applications.

MM was introduced with single magnetic phase by electroplating of a metallic nonmagnetic shell. There, the magnetoelastic anisotropy induced during the electroplating modified drastically the magnetic behavior of ferromagnetic nucleus.[14] More interesting is the case of MM with two magnetic phases, where additional magnetostatic coupling determines the magnetic behavior of the system.[15–20] The versatile fabrication process allows choosing a wide range of alloy compositions that enable playing with the magnetic character of each phase: soft core and hard shell or vice versa and where the relative thickness of each magnetic phase plays an important role in determining their magnetic interactions. They diversify the magnetic response of the MM at a high frequency involving interesting effects as asymmetric magnetoimpedance and multiabsorption ferromagnetic resonance.

This article revises most relevant magnetic properties of bimagnetic microwires focusing on: (I) biphase behavior and interphase magnetoelastic and magnetostatic interactions, (II) asymmetric magnetoimpedance and multiabsorption FMR effects, and (III) multilayer biphase microwires as sensing elements in various devices.

FABRICATION AND CHARACTERIZATION OF MULTILAYER BIMAGNETIC MICROWIRES

The biphase magnetic microwires are composed by a ferromagnetic nucleus, an intermediate glass layer, and a ferromagnetic outer shell (Fig. 1a). They are fabricated by the combination of ultrarapid solidification and electroplating techniques. The ferromagnetic nucleus covered by a Pyrex layer is obtained by the quenching and drawing method[3,7] (Fig. 1b). The diameter of the nucleus and thickness of the glass cover range between 1 μm and 20 μm. Due to the strong quenching rate of approximately 10^5 K/s, the ferromagnetic nucleus typically exhibits amorphous structures conferring soft magnetic properties. Three different kinds of magnetic alloys with soft behavior have been considered according to its saturation magnetostriction value: Fe-based ($\lambda_s = 10^{-5}$), Co-based ($\lambda_s = -10^{-6}$), and CoFe-based alloys with vanishing magnetostriction ($\lambda_s = -10^{-7}$). Several attempts were made to obtain microwires with harder magnetic behavior[21–23] using different compositions as CoFeCr, CoNiCu, and CoFeMo after suitable temperature treatment to promote the crystallization of magnetic phases with strong crystalline anisotropy. Others alloys (FeNdB, FePt, FePtNdB, FePd, and CoSm) were also explored; however, their saturation magnetization significantly decreases after the treatment at a high temperature. In this work, we show, as an example, results on FePt microwire after suitable thermal treatment: The transition from face-centered cubic (fcc) disorder to face-centered tetragonal (fct) ordered phase enhardens its magnetic behavior.[19,24]

An Au nanolayer (typically 30 nm thick) is grown on top of the glass surface using commercial sputtering system to serve as an electrode for the subsequent electroplating of the magnetic outer layer (Fig. 1c–e). Typically, two different magnetic alloys have been selected as magnetic outer layer: FeNi[10,24,25] and CoNi[15,17] with soft and hard magnetic behavior, respectively. The nominal composition of the alloys is tailored through the current

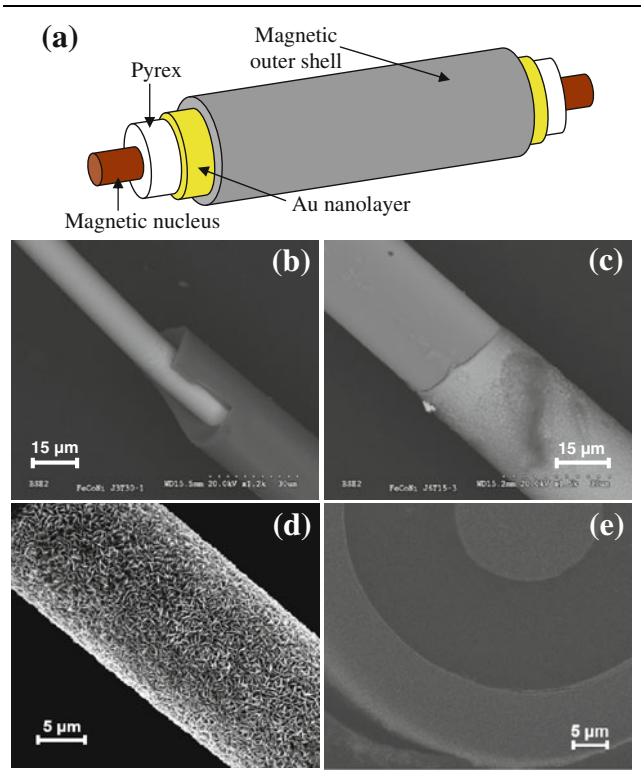

Fig. 1. (a) Scheme of multilayer microwire. SEM images of FeSiB/CoNi multilayer microwires: (b) FeSiB nucleus and glass cover, (c) glass layer and CoNi outer shell, (d) CoNi outer shell, and (e) cross-section view of the multilayer microstructure.

Table I. Magnetic nucleus radius (R_n), intermediate glass thickness (t_g), and magnetic outer shell thickness (t_{CoNi} or t_{FeNi}) of several biphase systems

	R_n (μm)	t_g (μm)	t_{CoNi}/t_{FeNi} (μm)
CoFe/CoNi	8.5	12	0–20
FeSiB/CoNi	6	9	0–20
FeSiBP/FeNi	7	12	0–7.5
CoFe/FeNi	7	2.5	0–6
FePt/FeNi	20	10	0–20

density of the electroplating, whereas the thickness is almost proportional to both time and current density. Other parameters affecting the quality and characteristics of the electroplating are the electrolyte temperature (optimal temperature of 40°C for these alloys) and the mechanical stirring.[26] In some cases, a circular magnetic field is used during FeNi electroplating to induce helical anisotropy.[27]

Here, we consider several biphase configurations: soft/hard ($Co_{67.06}Fe_{3.84}Ni_{1.44}Si_{14.47}B_{11.53}/Co_{90}Ni_{10}$ labeled as CoFe/CoNi and $Fe_{77.5}Si_{7.5}B_{15}/Co_{90}Ni_{10}$ labeled as FeSiB/CoNi),[14,15,17,18] soft/soft ($Co_{67.06}Fe_{3.84}Ni_{1.44}Si_{14.47}B_{11.53}/Fe_{20}Ni_{80}$ labeled as CoFe/FeNi and $Fe_{76}Si_9B_{10}P_5/Fe_{20}Ni_{80}$ labeled as FeSiBP/FeNi),[20,28] and hard/soft bimagnetic microwires ($Fe_{63}Pt_{27}Si_{10}/Fe_{20}Ni_{80}$ labeled as FePt/FeNi).[24] Their geometry characteristics are collected in Table I.

The amorphous microstructure of CoFeSiB and FeSiB alloys (typical amorphous halo at around 45°C has been confirmed by x-ray diffraction (not shown here).[19] FeNi and CoNi alloys show fcc and hexagonal close-packed crystalline structure.[19,24] FePtSi alloy exhibits an as-cast disordered fcc phase that transforms into to fct ordered phase after 15 min thermal treatment at 823 K.[19,24]

Nominal composition of different layers has been verified by EDS, microanalysis at surface, and x-ray fluorescence analysis of the full volume (not shown here).[19,20]

STATIC MAGNETIC PROPERTIES

Static and low-frequency magnetic properties were studied in a vibrating sample magnetometer (VSM) and by inductive fluxmetric techniques. Hysteresis loops were carried out at: (I) high field to analyze the biphase character and (II) low field (with demagnetized or premagnetized hard phase) to determine the magnetic interactions.

Major loops of biphase microwires present a typical two Barkhausen jumps behavior. In soft/hard systems (see Fig. 2a), a low field jump corresponds to magnetization reversal of the soft phase: CoFe, FeSiB, or FeNi, whereas the wider jump at higher field denotes the reversal process of harder phase takes place: CoNi or FePt. In CoFe/FeNi soft/soft system, both layers reverse magnetization at similar field range (FeNi presents higher permeability),[29] while in FeSiBP/FeNi, magnetization at the outer shell reverses first followed by the single Barkhausen jump of the nucleus.[28] The fractional section of each layer determines the amplitude of each jump and the coercivity of the biphase system.[15,30]

Minor loops, obtained after demagnetizing the hard phase, show practically only the magnetization process of the soft phase. Bistable magnetic behavior, with a single giant Barkhausen jump, is observed in positive-magnetostriction FeSiB nucleus for small-thickness external hard phase (Fig. 2b). Magnetization reversal occurs by depinning of a single domain wall from the closure structure at the end of the wire and its propagation.[31–33] Its domain structure is composed of a main axial core and a thinner radial outer shell as defined by the fabrication stresses, induced by quenching, drawing, and glass-cover. The relative volume of that axial domain increases with the glass cover thickness, producing a stronger longitudinal anisotropy and resulting in higher remanence M_r and switching field H_{sw}. The fractional radius R_c/R of the axial core reversed by domain wall propagation is given by $(R_c/R)^2 = (M_r/M_s)$.[3,34]

The presence of CoNi layer t_{CoNi} with increasing thickness induces internal stresses σ_{CoNi}. The corresponding magnetoelastic anisotropy deteriorates (progressive reduction of M_r and H_{sw}) and finally destroys the bistable behavior (see Fig. 2b, d) with a multidomain structure. According to the sign of magnetostriction λ_s, σ_{CoNi} is tensile axial or compressive transversal[30] in character and its strength (i.e., $\sigma_{CoNi} = 400$ MPa for $t_{CoNi} = 4.5$ μm) is estimated by:[35,36]

$$\sigma_{CoNi} = \alpha\left(H_{sw0}^2 - H_{sw}^2\right)/\gamma_{DW} \quad (1)$$

where H_{sw0} is the switching field of the single-phase microwire, γ_{DW} is the energy density stored at the domain wall, and α is a geometrical factor.

The magnetoelastic coupling was also analyzed in the alternative soft/hard CoFe/CoNi biphase system, where magnetostriction of the CoFe nucleus is small and negative,[17] and its domain structure is characterized by a main circumferential domain but containing an inner axial vortex structure.[37,38] In this case, the stresses induced by the CoNi external layer give rise to an effective axial anisotropy that is reflected in a progressive reduction with increasing layer thickness of the circumferential anisotropy field H_k and parallel increase of susceptibility χ (i.e., $H_k = 40$ A/m and $\chi = 11{,}000$ for $t_{CoNi} = 11$ μm). Such stresses (i.e., $\sigma_{CoNi} = 350$ MPa for $t_{CoNi} = 11$ μm) can be quantified by:

$$\sigma_{CoNi} = -\mu_0 M_s (H_{k0} - H_k)/3\lambda_s \quad (2)$$

where H_{k0} is the anisotropy field for the single phase CoFe glass-coated microwire.

The presence of the external layer together with that of the intermediate Pyrex layer is a source of stresses at the nucleus when temperature is

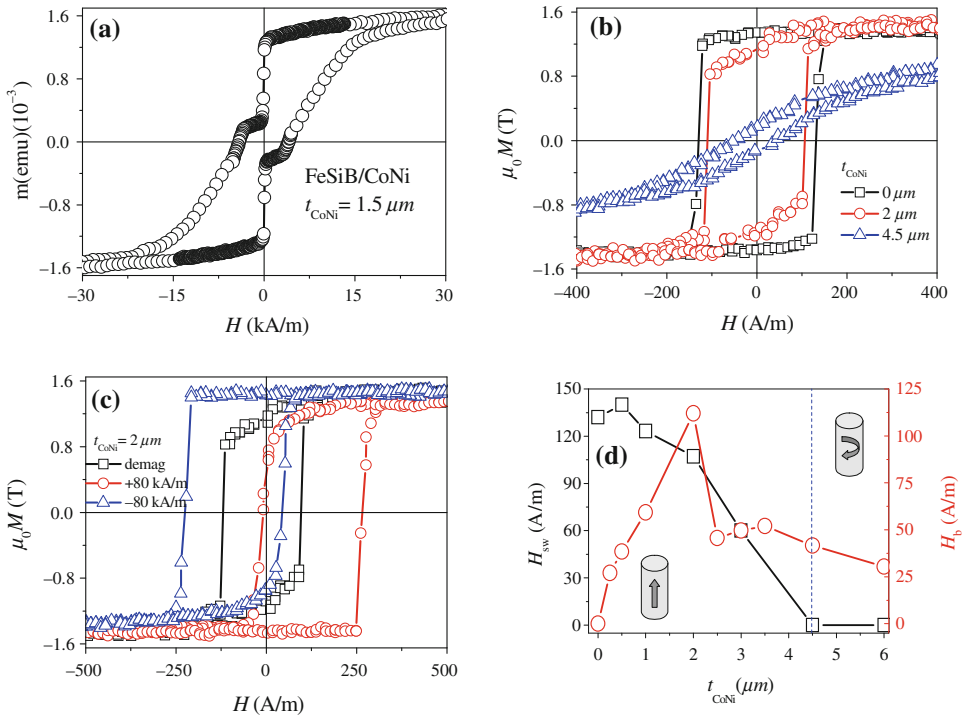

Fig. 2. Magnetic characterization for FeSiB/CoNi multilayer microwire: (a) major hysteresis loop showing bimagnetic phase nature, (b) increasing magnetoelastic anisotropy with CoNi thickness can destroy bistability, (c) premagnetizing history determines the bias field of the soft FeSiB core, and (d) evolution of switching H_{sw} and bias H_b fields with CoNi thickness.

modified (i.e., reduced). The thermoelastic stresses have been ascribed to the different thermal expansion coefficients of the metallic nucleus ($\alpha_n = 12 \times 10^{-6}$ K^{-1}) and the insulating glass cover ($\alpha_g = 3 \times 10^{-6}$ K^{-1}).[6,34,36] The evolution of magnetic properties with decreasing temperature is mainly determined by the glass layer, while the CoNi outer shell only modifies the initial magnetic structure. In CoFe/CoNi (FeSiB/CoNi) biphase systems, an increase of temperature reduces H_k (H_{sw}), that is, induces a magnetoelastic axial (circumferential) anisotropy. Therefore, the temperature change plays the same role as that of the CoNi thickness. Thermal stresses can be estimated using previous expressions taking into account the temperature dependence of the saturation magnetization, $M_s(T)$, and magnetostriction, $\lambda_s(T)$.[19]

Finally, in the case of hard/soft, FePt/FeNi biphase system, the magnetoelastic coupling during the electroplating of the soft magnetic phase is nearly negligible. The hard magnetic behavior of the nucleus is governed by the magnetocrystalline anisotropy of the $L1_0$ phase. On the other hand, temperature changes only affect the magnetic behavior of the FeNi outer shell, reducing remanence and coercivity decreasing temperature.[19,24]

Parallel to the magnetoelastic coupling, the magnetostatic interaction between magnetic phases can be relevant.[17,18] Its origin is found in the uncompensated magnetic charges at the ends of a premagnetized harder phase. They generate a magnetostatic field that adds to the applied field and biases the magnetic state of the soft phase. Figure 2c shows the minor hysteresis loops of the FeSiB/CoNi microwire (t_{CoNi} = 2 μm) when the hard phase is demagnetized and premagnetized at ±80 kA/m, respectively. The minor loop is shifted toward positive (negative) field when the CoNi layer has been magnetically saturated previously along positive (negative) orientation; that is, the bias field H_b is antiparallel to the magnetization of the hard phase. Moreover, premagnetized wires show asymmetric magnetization reversal. After positive premagnetization, the magnetization reversal in the lower branch (from negative to positive field) takes place fully by domain wall propagation while the upper branch (from positive to negative field), partial region reverses by rotation followed by domain wall propagation. Opposite behavior is found after negative premagnetization. This asymmetry can be explained by the inhomogeneity of the bias field being stronger in the region close to the uncompensated charges, and it forces such region to reverse by rotation instead of domain wall propagation.[18]

The magnetostatic bias depends strongly on the CoNi layer thickness. The evolution of H_b with t_{CoNi} is observed in Fig. 2d: The bias field increases with the thickness until critical t_{CoNi} = 2 μm, reaching maximum value of H_b = 112 A/m. The strong reduction of H_b for CoNi layer thickness higher than the critical value is correlated to a change of the magnetic structure in the FeSiB nucleus, as was

previously shown in the magnetoelastic analysis (Fig. 2b). There, bistability and the single axial domain disappear, leading to a change of magnetization easy axis from axial to circumferential direction. The same bias field evolution was observed in the alternative CoFeSiB/CoNi soft/hard biphase system, where a maximum H_b is measured for t_{CoNi} = 8 μm. The bias field was analytically modeled in terms of the geometry of the biphase system as:[39]

$$H_b = \frac{\pi M_s^e R_n R_T}{V} \int_0^\infty \frac{dk}{k^2} J_1(kR_n) \times \left[J_1(kR_T) - \frac{R_{GC}}{R_T} J_1(kR_{GC}) \right] (1 - \ell^{-kL}) \quad (3)$$

where $R_{GC} = R_n + t_g$ and V is the total volume of microwire. Calculations predict a strong H_b dependence on the thickness and length L of the hard magnetic outer shell and, particularly, that it reaches a maximum at a given critical thickness.

In the case of a soft/soft FeSiBP/FeNi biphase system, the switching field H_{sw} of the nucleus can be effectively controlled by the dipolar interaction with the FeNi outer shell through its geometry (thickness and length).[28] Finally, in the hard/soft FePt/FeNi biphase system with opposite magnetic configuration, the magnetostatic field is created by the hard nucleus and the shifted magnetization curves correspond to the FeNi softer outer shell. The bias field decreases strongly with FeNi thickness as was expected: Thicker FeNi layers are less affected by H_b.[24]

DYNAMIC MAGNETIC PROPERTIES

The study of magnetic properties of microwires has been extended to the radio and microwave frequency range for the case of soft/hard (CoFeSiB/CoNi and FeSiB/CoNi) and soft/soft (CoFeSiB/FeNi) biphase configurations. The presence of intermediate glass layer insulates electrically the internal and external metallic layers, and it allows the alternating current (AC) current excitation of the nucleus whose permeability will be affected by the magnetic interactions between metallic layers. Two phenomena are studied: GMI and FMR.

GMI consists in the huge changes in the wire impedance under the action of a static field or a stress. Its origin in ultrasoft magnetic systems relates with the variations of the skin effect[40–42] observed when a high-frequency current flows along the wire at the presence of static magnetic field. The penetration depth δ of the skin effect is given by $\delta = \sqrt{\rho/\pi\mu F}$, where for amorphous materials, the resistivity ρ is relatively high and $\delta < R_n$ at the MHz frequency F range. In GMI configuration, the AC current flows along the nucleus of the biphase wire inducing an AC circumferential field, exciting the circumferential permeability μ. After the action of a weak static field, permeability is modified and consequently the skin effect penetration depth, with the final variation of impedance.

The protocol of GMI measurement is the same as for static properties: The low-field GMI of the soft nucleus is measured with the hard magnetic layer in demagnetized or premagnetized state. Figure 3a illustrates the GMI effect of CoFe/CoNi MM for t_{CoNi} = 6 μm at 50 MHz. We observe a typical double peak behavior, where the maximum impedance is achieved at a static field balancing the circumferential anisotropy field, $H_k = 2K/\mu_0 M_s$. The magnetostatic bias field H_b shifts GMI curves toward positive (negative) field after positive (negative) premagnetization, as expected. In addition, the GMI curves show asymmetric behavior as a consequence of nonhomogeneous H_b. So, the peak with lower (higher) intensity is related to the region close to the ends (center) with stronger (weaker) H_b and lower (higher) susceptibility.[43] The evolution of the bias field with the frequency for selected t_{CoNi} is plotted in Fig. 3b. First, for small thickness, H_b is nearly constant in the whole frequency range, and it shows a progressive increase with t_{CoNi}. The data obtained from GMI technique are in agreement with static measurements for t_{CoNi} < 8 μm. We should note that the GMI technique only analyzes the surface impedance while magnetometric inductive techniques account for the whole magnetic

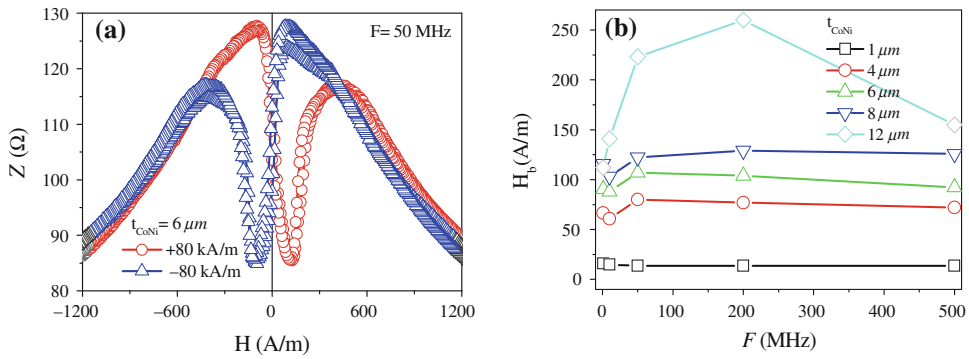

Fig. 3. (a) Asymmetric magneto-impedance for CoFe/CoNi multilayer microwire after premagnetizing to saturation in both directions. (b) Bias field evolution with frequency for different CoNi thickness.

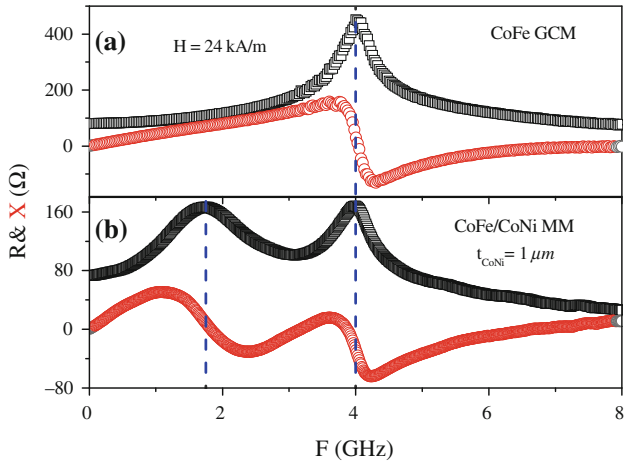

Fig. 4. Real R and imaginary X components of impedance as a function of frequency F for (a) CoFe GCM and (b) CoFe/CoNi MM at constant field of 24 kA/m.

volume of the samples. Concerning the influence of the magnetolastic coupling, the demagnetized GMI curves exhibit a transition from double to single peak as t_{CoNi} increases (not shown here). It denotes a change in the anisotropy from circular to axial.[43] Finally, in the case of FeSiB/CoNi biphase wires, the GMI effect of FeSiB is very small. Its transition from single (axial anisotropy) to double peak (circular anisotropy) GMI observed with increasing t_{CoNi} agrees with data in Fig. 2b.

The engineering microwave properties of amorphous GCM have been previously reported in both axial and circumferential radio frequency (RF) field configurations.[44–48] Here, we focus on the circular configuration (circumferential radial-dependent AC field generated by AC current flowing along the ferromagnetic nucleus). The impedance measurements have been performed using microstrip and transmission coaxial line techniques connected to a vector network analyzer. For more details in an experimental setup, see Refs. 43, 49, and 50.

The nonmagnetostrictive CoFe microwires present a single electromagnetic absorption in the frequency range between 1 and 6 GHz for saturating magnetic field in the range of kA/m. In turn, bistable FeSiB microwires show FMR at higher frequency range, 6–12 GHz, and even in the absence of any applied static field, an effect that is labeled natural FMR, in which the role of saturating field is played by the strong axial anisotropy field.[50,51]

The presence of a second hard phase modifies the microwave frequency response. Figure 4 illustrates the impedance spectra (Real and Imaginary components) for single phase CoFe GCM (Fig. 4a) and biphase CoFe/CoNi MM with t_{CoNi} = 1 μm at constant field of 24 kA/m. The main resonance, FMR1, at around 4 GHz corresponds to the excitation of CoFe. The CoNi layer introduces a second peak at lower frequency FMR2, 1.75 GHz.[50]

The impedance spectra of FeSiB/CoNi MM in Fig. 5a show a third absorption peak, labeled in principle as FMR3, at an intermediate frequency between FMR1 and FMR2. To get deeper information about the origin of the absorption phenomena, experimental data have been fitted to the Kittel relation[52] for macrospin approach. Note that the model for a cylinder is not valid because of the presence of the strong skin effect, and we have to consider a hollow cylinder tube being the model for thin plate more suitable.[48] In the particular case of $M_s \gg (H + H_k)$, the evolution of FMR frequency F_r with static applied field H is given by:

$$F_r = \frac{\gamma\mu_0}{2\pi}\sqrt{(H + H_k)M_s} \quad (4)$$

where γ is the gyromagnetic factor. From the fitting, we can evaluate the saturation magnetization M_s and the anisotropy field H_k. Figure 5b depicts the square absorption frequencies as a function of H for a single-phase FeSiB microwire and FeSiB/CoNi biphase microwires. FMR, FMR1, and FMR3 curves show similar M_s value (i.e., slope) close to the expected value obtained from static VSM data, $\mu_0 M_s$ = 1.55 T. A remarkable difference is found when extrapolating the two curves at F = 0. FMR and FMR1 curves show positive extrapolated field, H_k = 3 kA/m (i.e., axial anisotropy), while for FMR3, the extrapolated negative value H_k = −18 kA/m denotes a circumferential anisotropy. FMR2 curve presents an anomalous small slope for which Kittel relationship is no longer valid.[29,53] The origin of FMR2 absorption in CoFe/CoNi and FeSiB/CoNi has been correlated to a capacitance effect between the metallic layers, which depends on the Pyrex thickness.[29] CoNi absorption is not well defined owing to the lack of magnetic saturation due to its harder character. Multipeak electromagnetic absorption was observed in soft/soft CoFeSiB/FeNi MM, where FMR3 was ascribed to the excitation of FeNi outer shell.[53,54]

TECHNOLOGICAL APPLICATIONS

Engineering Sensing Applications

Many applications of magnetic amorphous microwires as sensing element have been proposed during the last 30 years due to their unique magnetic properties. In microwires with high magnetostriction λ_s, most of applications are related to magnetic bistability where sharp voltage is induced in pick-up coils during magnetization reversal, as for example in switchers, rotation counters, position and velocity sensors, security systems sensors, or identification magnetic tag.[55–57] Magnetostrictive microwires are also proposed in delay lines and sound velocity sensors,[58] digitizers,[59] direct current (DC) current sensor,[60] noncontact torsion sensors, thermoelastic sensor, viscometer,[61] and magnetoelastic sensor for signature identification.[62] Microwires with vanishing λ_s are among the softest

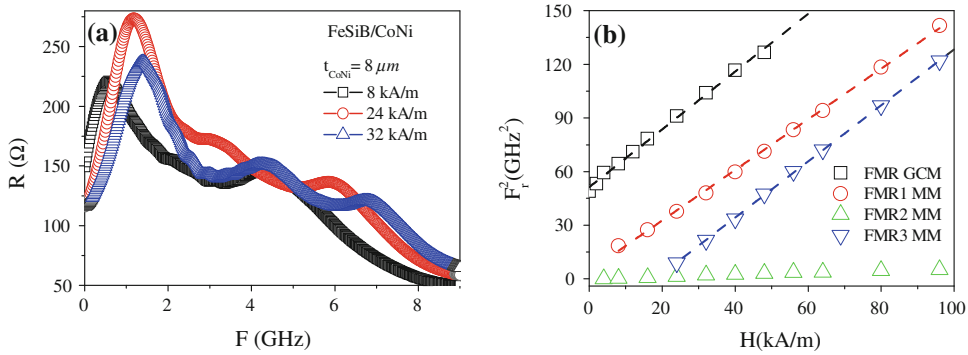

Fig. 5. (a) Multipeak absorption for FeSiB/CoNi biphase microwires under various static applied fields. (b) Evolution of FMR peaks F_R with applied field, H: Linear fit of F_r^2 versus H for FeSiB GCM, and FeSiB/CoNi MM.

magnetic materials with a great potential for sensor devices: (I) magnetic tip in SP-STM,[63] (II) GMI-based sensors as in GPS applications,[64] (III) stress impedance sensors for biomedical applications,[64,65] and (IV) electromagnetic absorption for radar devices.[66] Very recently, a multifunctional (temperature and humidity) sensor based on hybrid magnetic microwire/sol–gel TiO_2 coating nanostructure has been proposed.[67] Multilayer microwires can be successfully employed in various sensing applications. Here, we focus on two particular developments, namely, a multifunctional sensor and the processing to achieve optimal elements for orthogonal flux-gate sensor.

Multifunctional Sensors Based in Biphase Microwires

A novel type of multifunctional sensor device was proposed where the sensing element is a CoFe/CoNi MM.[68,69] The magnetization of the nearly nonhysteretic soft magnetic CoFe nucleus is very sensitive to small changes of environment conditions (i.e., temperature, stress, and magnetic field), while the CoNi hard outer shell plays a complementary role to control its magnetic state. Two operational principles are used: (I) the modified small angle magnetization rotation (MSAMR) technique (temperature and mechanical stress sensor)[70] and (II) the asymmetric magnetoimpedance (AMI) (position and magnetic field sensor).

The MSAMR is based on the classical SAMR method introduced by Narita,[71] which was used for many years to quantify almost vanishing λ_s. This method required the axial magnetic saturation of a soft core (i.e., by means of a DC axial field created by a solenoid), and the application of small amplitude AC transverse field (i.e., by means of Helmholtz coils or a current flowing along the sample[72]) to induce small-amplitude oscillations of the magnetization. The amplitude of oscillations depends on the static field or mechanical stress to be sensed typically by a pick-up coil wounded around the wire.

In the MSAMR method, the saturating field and stress are provided by the stray field and the stress introduced by the hard phase.[68,69] The extremely simple scheme is shown in Fig. 6a. The MM sensor element was connected to an LCR analyzer that, at the same time, procured the flow of AC current through the wire nucleus and gave an impedance reading of the nucleus itself.

Figure 6b depicts the temperature-induced change of fractional inductance of the core. Such variation is magnetoelastically induced by the stresses arising from the different thermal expansion coefficient of the multilayer microwire (see the "Static Magnetic Properties" section). We observe a noticeable increase (6.3%/°C) of inductance around human body temperature, which is compared to negligible effect in single phase wire. Also, the temperature sensor shows a fast and efficient response (time constant $\tau = 0.7$ s for $\Delta T = 25$°C.[68,69,73] In addition, the sensor can be used simultaneously to sense tensile (Fig. 6c) and torsional (Fig. 6d) stresses profiting of the suitable magnetostrictive behavior of these microwires.[74]

A second method makes use of the AMI effect (see the "Dynamic Magnetic Properties" section). Single-phase CoFe GCM presents symmetric double-peak behavior, while in asymmetric GMI, we profit of the large variation of impedance with static magnetic field as well as its linear dependence facilitates the signal recording. Several alternatives have been proposed to achieve AMI: (I) using a pulse bias circuit,[64] (II) applying DC current,[75] and (III) analyzing the diagonal component of impedance using pick-up coil wounded around microwire.[76] These methods request additional electronics, sometimes a higher power consumption and difficulties in the positioning of the magnet. In the case of biphase microwires, the stray field of the CoNi outer shell produces straight such AMI response around zero static field (see Fig. 6e) without additional electronic components.[43] The optimum result, with linear impedance change around 50%, was found in CoFe/CoNi MM with $t_{CoNi} = 4$ μm.

Functional sensors based on biphase systems have been tested for biomedical applications in monitoring the cardiorespiratory activity and rapid

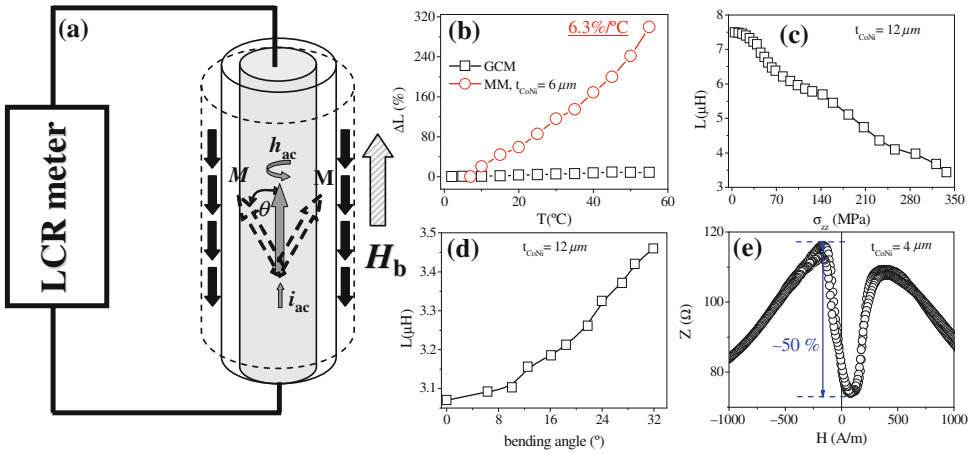

Fig. 6. (a) Multifunctional sensing elements based on CoFe/CoNi MM: (b) temperature, (c) tensile stresses, (d) torsion, and (e) position and magnetic field sensors. Amplitude and frequency of AC current were set in 100 mV and 1 MHz, respectively, but for magnetic field sensor, 50 MHz.

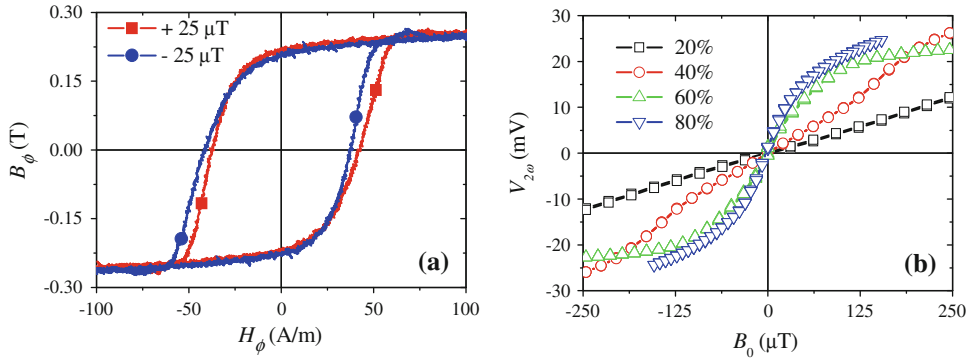

Fig. 7. (a) Shifted circular hysteresis loops under positive and negative axial fields evidencing the presence of helical anisotropy and (b) second harmonic voltage as a function of longitudinal field obtained in a torsion-induced helical anisotropy wire for a range of working cycles.

eye movement (REM) phases.[77,78] In general, sensor devices based in biphase microwires present advantages as high sensitivity, quick response time, simplified and robust technology, reduced fabrication cost, easy integration in miniaturized devices, and a multifunctional character.

Fluxgate Based in Multilayer Microwire

Fluxgates are widely employed very sensitive magnetic field sensors.[79] They are usually classified into parallel and orthogonal ones depending on the relative orientation of excitation and sensed fields. While many applications are based on parallel fluxgates because of their good properties, orthogonal fluxgates have been recently rediscovered thanks to the use of magnetic microwire as core instead of bulk cylinders.[80]

The sensing element consists of a magnetic microwire where an AC current flows along the wire, generating the circumferential excitation field that avoids the need of any excitation coil (a pickup coil is still necessary to measure the variation of longitudinal field). Glass-coated bimetallic microwires offer an additional advantage. They are composed of a Pyrex-coated Cu microwire core covered by a relatively thin soft magnetic material layer, typically Permalloy as in previous biphase microwires. The Cu core carries the AC current (the thin Pyrex coat insulates both metallic layers) that results in the circular magnetic saturation of Permalloy.[27]

The microwire can work in coil-less fluxgate mode (i.e., without the need of any coil) if the magnetic outer layer exhibits helical anisotropy. In that case, under an applied longitudinal field to be sensed, circular magnetization changes owing to the helical anisotropy. There, an output signal is received from the ends of the external Py layer which is proportional to changes in the circular magnetization of the wire. Such helical anisotropy can be achieved by mechanically twisting the wire. However, that method shows a sensor stability drawback. An alternative technique has been proposed where an intrinsic helical anisotropy is induced during the Py electroplating by (I) a helical magnetic field (superposition of a longitudinal field generated by a

Helmholtz coil and a circumferential field produced by a DC current flowing through the Cu core) (see Fig. 7a)[81,82] and (II) an applied torque to the multilayer microwire that is afterward relieved so keeping a helical backstress (see Fig. 7b).[20,83] In both cases, second harmonics signal evolves linearly with magnetic field in a range that can be tuned by Py electroplating parameters.

FINAL CONCLUSIONS AND PERSPECTIVES

An overview on the new family of magnetic microwires with multilayer bimagnetic characteristics has been presented. That includes preparation and processing, static and dynamic magnetic properties, and some examples of their application in sensor devices. Regarding the preparation procedures, we should emphasize that to achieve the multilayer character several complementary techniques are employed, namely, quenching and drawing (precursor glass-coated magnetic/metallic core microwire), sputtering (Au metallic intermediate nanolayer), and electroplating (magnetic external microtube). Such techniques enable the preparation of layers with different soft/hard magnetic character allowing us to tune the properties of the biphase microwires. The structure/magnetic characteristics of individual phases can be optimized by specific thermal treatment processing to (I) grow new structural phase with hard magnetic character at the magnetic core (simple thermal treatment) or (II) induce suitable helical anisotropy at the magnetic shell (helical magnetic field annealing or torsion annealing). Very recently, alternative hard magnetic outer shells of CoPt and CoPtCu have been prepared by direct sputtering onto glass-coated microwire and subsequently heat treated to grow highly anisotropic $L1_0$ phase, achieving a hard phase coercivity of 10 kA/m.[84]

The magnetic behavior of biphase microwires is essentially characterized by two main magnetization reversal processes corresponding to the individual phases, their respective magnetization reversal and coercivity mechanisms being determined by their soft/hard nature. Different magnetic configurations have been explored: soft (nucleus)/hard (outer shell), hard/soft, and soft/soft. However, one can take advantage of the magnetic interactions between phases to play in a relevant way to suit the soft magnetic core behavior: For example, it can be biased through the hard phase stray fields, or magnetic bistability can be either destroyed or generated through the magnetoelastic anisotropy induced by the external phase. Apart from the soft/hard magnetic nature of each magnetic phase, an appropriate tuning of that behavior can be achieved by adequate thickness tailoring of each layer (i.e., intermediate Pyrex glass and/or external magnetic layer).

The study of fundamental aspects of biphase microwires still offers some open questions. In particular, temperature-related effects seem of major relevance and should be studied in detail. High temperature induces reversible changes in the magnetic anisotropy, but also it can enable irreversible atomic diffusion between interlayers.[85] In turn, low-temperature measurements allow us to get deeper information on intrinsic magnitudes (spin waves, magnetic anisotropy, and magnetic interactions).[86] While the different thermal expansion coefficients of layers have been used to interpret the intrinsic magnetoelastic characteristics of the microwires, it also offers an interesting inverse effect where temperature changes gives rise to mechanical oscillations.[87]

This new family of multilayer microwires was obtained after years of research around the development of new magnetic materials to be used as sensing core elements in sensor devices. The possibility to control the reversal magnetization of the soft phase, through magnetic couplings induced by the hard phase, makes this microwire ideal candidate in sensor technologies. Here, we have shown a few examples where multilayer microwires are employed as elements in multifunctional (temperature/tensile stress and torsion/position) sensors based in specific properties (coil-less small angle magnetization rotation and asymmetric magnetoimepdance), or in coil-less orthogonal fluxgates.

The versatility of properties and of their tailoring makes multilayer bimagnetic microwires very useful to the scientific and technological magnetic community. The search for new processing of microwires to optimize their properties is open, and imaginative alternatives will offer new opportunities in the near future.

ACKNOWLEDGEMENTS

The work was supported by the Spanish Ministries of Science and Technology (last Project MAT2010-20798), the European Communities under Project B-Sens Growth GRD1-2001-40725, and Czech-Spain bilateral framework Programs P2008CZ0020 and P2006CZ0020, and Morocco-Spain bilateral Framework Program P2005MA0112. J. Torrejon and G. Infante are thankful to MEC for Ph.D. Fellowships. The authors deeply acknowledge very fruitful discussions and hospitality at their Research Centers to Ludek Kraus, Larissa Panina, Juan Escrig, Dora Altbir, Rastislav Varga, Mohamed R. Britel, Mattia Butta, and Pavel Ripka.

REFERENCES

1. F.E. Luborsky, *Amorphous Metallic Alloys* (London: Butterworths, 1983).
2. K. Handrich and S. Kobe, *Amorphe Ferro- und Ferrimagnetika* (Weinheim: Physik-Verlag, 1980).
3. M. Vazquez, *Handbook of Magnetism and Advanced Magnetic Materials* (Chichester: Wiley, 2007), p. 2193.
4. M.E. McHenry, M.A. Willard, and D.E. Laughlin, *Prog. Mater Sci.* 44, 291 (1999).
5. A. Zhukov and V. Zhukova, *Magnetic Properties and Applications of Ferromagnetic Microwires with Amorphous*

and Nanocrystalline Structure (Hauppauge, NY: Nova Science Publishers, Inc., 2009), pp. 11788, 162.
6. H. Chiriac and T.A. Ovari, *Prog. Mater Sci.* 40, 333 (1996).
7. A. Zhukov, J. Gonzalez, M. Vazquez, V. Larin, and A. Torcunov, *Encyclopedia of Nanoscience and Nanotechnology*, Vol. 6, ed. H.S. Nalwa (Valencia, CA: American Scientific Publishers, 2004), p. 365.
8. M. Vazquez, H. Chiriac, A. Zhukov, L. Panina, and T. Uchiyama, *Phys. Stat. Sol. A* 238, 493 (2011).
9. J.P. Sinnecker, J.M. Garcia, A. Asenjo, M. Vazquez, and A. Garcia-Arribas, *J. Mater. Res.* 15, 751 (2000).
10. J.M. Garcia, A. Asenjo, M. Vazquez, A.M. Yakunin, A.S. Antonov, and J.P. Sinnecker, *J. Appl. Phys.* 89, 3888 (2001).
11. M. Vázquez, L. Kraus, K. Pirota, G. Badini, and J. Torrejón, *J. Non-Cryst. Solids.* 353, 763 (2007).
12. P. Mendoza-Zelis, F. Sanchez, and M. Vazquez, *J. Appl. Phys.* 101, 034507 (2007).
13. L. Kraus, K. Pirota, J. Torrejón, and M. Vázquez, *J. Appl. Phys.* 101, 063910 (2007).
14. K. Pirota, M. Hernández-Vélez, D. Navas, A. Zhukov, and M. Vázquez, *Adv. Funct. Mater.* 14, 266 (2004).
15. K. Pirota, M. Provencio, K. García, P. Mendoza, M. Hernandez-Velez, and M. Vázquez, *J. Magn. Magn. Mater.* 290, 68 (2005).
16. G.A. Badini-Confalonieri, J. Torrejón, K.R. Pirota, and M. Vázquez, *Magnetic Materials: Current Topics in Amorphous Wires, Hard Magnetic Alloys, Ceramics, Characterization and Modelling* (Kerala: Research Sign Post, 2007), Chap. 3.
17. J. Torrejón, G. Badini, K. Pirota, and M. Vázquez, *Acta Mater.* 55, 4271 (2007).
18. G. Badini-Confalonieri, G. Infante, J. Torrejón, and M. Vázquez, *J. Magn. Magn. Mater.* 320, 2443 (2008).
19. Jacob Torrejon (Ph.D. thesis, Autonomous University, Madrid, 2009).
20. German Infante, (Ph.D. thesis, Autonomous University, Madrid, 2010).
21. K.Y. Wang, D.X. Chen, J. Arcas, V. Larin, J. Velazquez, M. Vazquez, and A. Hernando, *J. Phys.: Condens. Matter* 9, L573 (1997).
22. A. Zhukov, J. Gonzalez, J.M. Blanco, M. Vazquez, and V. Larin, *J. Mater. Res.* 15, 2107 (2000).
23. H. Chiriac, F. Borza, and I. Murgulescu, *Mater. Sci. Forum* 373, 245 (2001).
24. J. Torrejón, G. Badini-Confalonieri, and M. Vázquez, *J. Appl. Phys.* 103, 07E712 (2008).
25. R.S. Beach, N. Smith, C.L. Platt, F. Jeffers, and A.E. Berkowitz, *Appl. Phys. Lett.* 68, 2753 (1996).
26. M. Schlesinger and M. Paunovic, *Modern Electroplating* (New York: Wiley, 2000).
27. M. Butta, P. Ripka, G. Infante, G.A. Badini-Confalonieri, and M. Vázquez, *IEEE Trans. Magn.* 45, 4443 (2009).
28. G. Infante, G.A. Badini-Confalonieri, R.P. del Real, and M. Vázquez, *J. Phys. D* 43, 345002 (2010).
29. R. El Kammouni, G. Infante, J. Torrejon, M.R. Britel, J. Brigui, and M. Vazquez, *Phys. Stat. Sol. A* 208, 520 (2011).
30. J. Torrejón, G. Infante, K.J. Merazzo, and G.A. Badini-Confalonieri, *IEEE Trans. Magn.* 44, 3942 (2008).
31. R. Varga, K.L. Garcia, M. Vazquez, and P. Vojtanik, *Phys. Rev. Lett.* 94, 017201 (2005).
32. M. Vazquez, G.A. Basheed, G. Infante, and R.P. del Real, *Phys. Rev. Lett.* 108, 037201 (2012).
33. J. Ye, R.P. del Real, G. Infante, and M. Vazquez, *J. Appl. Phys.* 113, 043904 (2013).
34. H. Chiriac, T.A. Ovari, and G. Pop, *Phys. Rev. B* 52, 10104 (1995).
35. P. Aragoneses, J.M. Blanco, L. Dominguez, J. Gonzalez, A. Zhukov, and M. Vazquez, *J. Phys. D* 31, 3040 (1998).
36. R. Varga, K.L. García, A. Zhukov, P. Vojtanik, and M. Vázquez, *Appl. Phys. Lett.* 83, 2620 (2003).
37. J. Torrejon, A. Thiaville, A.L. Adenot-Engelvin, M. Vázquez, O. Acher, and J. Mag, *Magn. Mater.* 323, 283 (2011).
38. J. Torrejon, A. Thiaville, A.L. Adenot-Engelvin, and M. Vázquez, *J. Magn. Magn. Mater.* 333, 144 (2013).
39. J. Escrig, S. Allende, D. Altbir, M. Bahiana, G. Badini, J. Torrejón, and M. Vázquez, *J. Appl. Phys.* 105, 023907 (2009).
40. L.V. Panina and K. Mohri, *Appl. Phys. Lett.* 65, 1189 (1994).
41. R.S. Beach and A.E. Berkowitz, *Appl. Phys. Lett.* 64, 3652 (1994).
42. M. Knobel, M. Vazquez, and L. Kraus, *Giant Magnetoimpedance* (Amsterdam: Elsevier, 2003), p. 497.
43. J. Torrejón, M. Vázquez, and L.V. Panina, *J. Appl. Phys.* 105, 033911 (2009).
44. D. Menard and A. Yelon, *J. Appl. Phys.* 88, 322 (2000).
45. O. Reynet, A.-L. Adenot, S. Deprot, O. Acher, and M. Latrach, *Phys. Rev. B* 66, 094412 (2002).
46. S.E. Lofland, H. Garcia-Miquel, M. Vazquez, and S.M. Bhagat, *J. Appl. Phys.* 92, 2058 (2002).
47. D.P. Makhnovskiy and L.V. Panina, *J. Appl. Phys.* 93, 4120 (2003).
48. L. Kraus, G. Infante, Z. Frait, and M. Vazquez, *Phys. Rev. B* 83, 174438 (2011).
49. D. Menard, M. Britel, P. Ciureanu, A. Yelon, V.P. Paramonov, A.S. Antonov, P. Rudkowski, and J.O. Ström-Olsen, *J. Appl. Phys.* 81, 4032 (1997).
50. J. Torrejón, G. Badini, and M. Vázquez, *J. Appl. Phys.* 106, 023913 (2009).
51. A.N. Antonenko, S.A. Baranov, V.S. Larin, and A.V. Torcunov, *J. Mater. Sci. Eng. A* 247, 248 (1997).
52. C. Kittel, *Introduction to Solid State Physics* (New York: Wiley, 1996), Chap. 16, p. 503.
53. J. Torrejón, G. Badini, and M. Vázquez, *J. Phys. D* 43, 145001 (2010).
54. R. El Kammouni and M. Vazquez, *IEEE Trans. Magn.* 49, 34 (2013).
55. G. Rauscher and C. Radeloff, *Magnetic Sensors*, ed. R. Boll and K.J. Overshott (Weinheim: Wiley VCH, 1989), p. 315.
56. K. Mohri, *IEEE Trans. Magn.* 20, 942 (1994).
57. A. Hernando, A. Zhukov, M. Vázquez, V. Larin, A. Torkunov, and A. Antonenko, ES patent 9601993 (1993).
58. E. Hristoforou and D. Niarchos, *J. Magn. Magn. Mater.* 116, 177 (1992).
59. T. Meydan and M.S. Elshebani, *J. Magn. Magn. Mater.* 112, 344 (1992).
60. E. Pulido, R.P. del Real, F. Conde, G. Rivero, M. Vázquez, and A. Hernando, *IEEE Trans. Magn.* 27, 5241 (1991).
61. M. Vázquez, F. Castaño, T.A. Ovari, V. Raposo, and A. Hernando, *Sens. Actuator. A* 91, 112 (2001).
62. A. Zhukov, M. Vázquez, and J.M. Beneytez, *J. Phys. IV* 8, 763 (1998).
63. W. Wulfhekel, H. Ding, W. Lutzke, G. Steirl, M. Vázquez, P. Marín, and A. Hernando, *Appl. Phys. A* 72, 463 (2001).
64. K. Mohri, T. Uchiyama, L.P. Shen, C.M. Cai, L.V. Panina, Y. Honkura, and M. Yamamoto, *IEEE Trans. Magn.* 38, 3063 (2002).
65. G. Kurlyandskaya and V. Levit, *Biosen. Bioelectron.* 20, 1611 (2005).
66. S.A. Baranov, *Tech. Phys. Lett.* 43, 122 (1998).
67. C. Gomez-Polo, J. Soto-Armañanzas, J. Olivera, J.I. Perez-Landazabal, S. Larumbe, M.A. Miranda, C.A. de la Cruz, I. Mendizabal, S.A. Korili, and A. Gil, *Ind. Eng. Chem. Res.* 52, 3787 (2013).
68. M. Vazquez, H. Pfützner, K. Pirota, G. Badini, and J. Torrejón, EU patent PCT/ES2005/070173 (2006).
69. J. Torrejón, G. Badini, K. Pirota, and M. Vázquez, *Sens. Lett.* 5, 153 (2007).
70. J. Torrejón, G. Badini, K. Pirota, and M. Vázquez, *J. Magn. Magn. Mater.* 316, 575 (2007).
71. K. Narita, *IEEE Trans. Magn.* 16, 435 (1980).
72. A. Hernando, M. Vazquez, V. Madurga, E. Ascasibar, and M. Liniers, *J. Magn. Magn. Mater.* 61, 39 (1986).
73. J. Torrejón, K.R. Pirota, G.A. Badini-Confalonieri, and M. Vázquez, *Sens. Lett.* 7, 1 (2009).
74. A. Zhukov, J.M. García Beneytez, and M. Vazquez, ES patent 9600172 (1996).

75. L. Kraus, Z. Freit, K. Pirota, and H. Chiriac, *J. Magn. Magn. Mater.* 254–255, 399 (2003).
76. S. Sandacci, D. Makhnovsky, L. Panina, K. Mohri, and Y. Honkura, *IEEE Trans. Magn.* 40, 3505 (2004).
77. H. Pfützner, E. Kaniusas, J. Kosel, L. Mehnen, T. Meydan, M. Vázquez, M. Rhon, A.M. Merlo, and B. Marquardt, *Sens. Actuators* 129, 154 (2006).
78. E. Kaniusas, H. Pfützner, L. Mehnen, J. Kosel, J.C. Tellez-Blanco, G. Varoneckas, A. Alonderis, T. Meydan, M. Vázquez, M. Rhon, A.M. Merlo, and B. Marquardt, *IEEE Sens. J.* 6, 819 (2006).
79. F. Primdhal, *J. Phys. E: Sci. Instrum.* 12, 241 (1979).
80. I. Sasada, *J. Appl. Phys.* 91, 7789 (2002).
81. M. Butta, P. Ripka, G. Infante, G.A. Badini-Confalonieri, and M. Vazquez, *IEEE Trans. Magn.* 46, 2562 (2010).
82. M. Vazquez, G. Badidni, G. Infante, M. Butta, and P. Ripka, patent PCT/ES2009/070417 (2009).
83. M. Butta, P. Ripka, M. Vazquez, G. Infante, and L. Kraus, *Sens. Lett.* (2013, in press).
84. F. Borza, S. Corodeanu, N. Lupu, and H. Chiriac, *J. Alloy. Compd.* 554, 150 (2013).
85. V. Rodionova, A. Nikosin, J. Torrejon, G. Badidni-Confalonieri, N. Perov, and M. Vazquez, *IEEE Trans. Magn.* 47, 3787 (2011).
86. V. Morin, R. El Kammouni, R.P. del Real, and M. Vazquez, unpublished work (2013).
87. V. Kolesar, R. El Kammouni, M. Kubliha, V. Labas, and M. Vazquez, unpublished work (2013).